$MgO/MgCl_2/TiCl_4$ Core-Shell Catalyst for Establishing Structure-Performance Relationship in Ziegler-Natta Olefin Polymerization

Patchanee Chammingkwan, Vu Quoc Thang, Minoru Terano and Toshiaki Taniike*

School of Materials Science, Japan Advanced Institute of Science and Technology, 1-1 Asahidai, Nomi, Ishikawa, 923-1292, Japan

Corresponding author

Assoc. Prof. Dr. Toshiaki Taniike

TEL: +81-761-51-1630, FAX: +81-761-51-1635, E-mail: taniike@jaist.ac.jp

Keywords: Ziegler-Natta polymerization, structure-performance relationship, core-shell, nanoparticle, α_S-plot

Summary

Recently we successfully established the first structure-performance relationships between the catalyst surface area and propylene polymerization activity using novel $MgO/MgCl_2/TiCl_4$ core-shell catalysts with non-porous and non-fragmentable features. In the present paper, we have addressed the physical and chemical natures of these novel model catalysts in comparison with typical Ziegler-Natta catalysts, by means of comprehensive characterization and analyses. It was clarified that the $MgO/MgCl_2/TiCl_4$ core-shell catalysts offer an ideal and powerful tool to address relationships between the support architectures and polymerization performance, which had been long un-clarified.

1. Introduction

Since the memorial discovery by Karl Ziegler and Gulio Natta in 1953 and 1954, the heterogeneous Ziegler-Natta (ZN) catalyst has become indispensable catalyst for the industrial production of polyolefins for more than half century. A numerous amount of research have been undertaken during the past 60 years to attain molecular-level knowledge on the catalyst structure as well as on the polymerization mechanism. As a consequence, the nature of active site has been elucidated to some extent. For instance, the adsorption site of $TiCl_4$ occurs on the lateral surfaces of $MgCl_2$ such as the (110) and (104) cuts exposing under-coordinated Mg^{2+} ions on the surfaces[1]. In contact with alkyl aluminum cocatalyst, supported $TiCl_4$ is converted to an active site that equips a coordinative vacancy for incoming monomer olefin and a Ti-carbon bond as a growing chain. The polymerization initiates from the coordination of olefin monomer followed by migratory insertion of the coordinated monomer into the Ti-carbon bond as described by the Cossee-Arlman mechanism[2]. Ethylene can be polymerized irrespective of the oxidation state of Ti species with the tendency of higher molecular weight for a lower oxidation state of Ti[3]. On the contrary, Ti^{2+} species is inactive for polymerization of α-olefin. Internal donor play important roles in stabilizing primary crystallites of $MgCl_2$[4] and in drastically improving the stereoselectivity in propylene polymerization through its coadsorption with a Ti center.[5-7]

One of the breakthroughs in the heterogeneous ZN catalyst is the discovery of highly active catalyst by utilizing activated $MgCl_2$ as the catalyst support. The activation can be conducted by either mechanical grinding of anhydrous $MgCl_2$ or chemical treatment of $MgCl_2$-alcohol adduct or magnesium alkoxide with a chlorinating agent. Microscopically, the activation causes the disordering in the stacking of Cl–Mg–Cl layers along the [001] axis as well as the

reduction of the crystal dimensions of $MgCl_2$. Macro- and mesoscopically, catalyst particles consist of hierarchical but irregular agglomeration of primary structural units, which bears a wide variety of intra-particle porosity from macro to micro. The hierarchy structure is important to control the polymerization activity over hours: polymerization-induced fragmentation breaks up the porosity and thus continuously supplies new active sites which are originally hidden inside pores. However, such the complexity makes it extremely demanding to quantitatively examine latent correlations between the support architectures and polymerization performance of typical ZN catalysts. Gerbasi et al.[8] examined the correlation between the ethylene polymerization activity and the grinding time for a $TiCl_4/MgCl_2$ catalyst. The activity was correlated with the structural disorder of $MgCl_2$ support rather than the catalyst surface area.[8] Margio et al.[9] employed several ZN catalysts prepared from $MgCl_2$-alcohol adduct to study the correlation between the propylene polymerization activity and the catalyst surface area. While the activity was never correlated with the BET surface area, some level of correlation was found for the surface area obtained by small-angle X-ray scattering technique. Recently, we have applied the α_S-plot method to investigate the validity of the BET surface area for $MgCl_2$-alcohol adduct-based and $Mg(OEt)_2$-based ZN catalysts.[10] The α_S-plots revealed the presence of two classes of micropores, which disabled the evaluation of the physically meaningful BET surface area for typical ZN catalysts.

To overcome the above-mentioned problems for the support architectures, a model catalyst approach has been successfully employed by our group[11]: A series of $MgO/MgCl_2/TiCl_4$ core-shell catalysts with a variety of surface areas were fabricated. Non-porous particles with a non-fragmentable MgO crystal core enabled us not only to systematically alter the catalyst surface area by changing the particle size but also to establish the first clear

proportional relationship between the propylene polymerization activity and the BET surface area.

The present paper delivers full characterization results for the $MgO/MgCl_2/TiCl_4$ core-shell catalysts, including X-ray diffraction (XRD), α_S-plot analysis in nitrogen adsorption, X-ray photoemission spectroscopy (XPS) and polymerization kinetics, in order to clarify novel physicochemical properties of the model catalysts.

2. Experimental Part

Preparation of MgO nano-crystals

MgO nano-crystals were prepared using a sol-gel method according to the procedure described in literature.[12] Magnesium nitrate hexahydrate ($Mg(NO)_3.6H_2O$), and oxalic acid dihydrate ($(COOH)_2.2H_2O$), purchased from Wako Pure Chemical Industries, Ltd. were separately dissolved in ethanol. Subsequently, two precursors were mixed together at the molar ratio of 1:1 and vigorously stirred for 12 h. After completion, dense white gel of magnesium oxalate precursor was dried at 100ºC for 24 h before calcination in air to obtain MgO nano-crystals.

Preparation of $MgO/MgCl_2/TiCl_4$ catalyst

MgO nano-crystal powder was preliminarily dehydrated at 130°C under nitrogen flow for 6 h. 30 ml of $TiCl_4$ (purchased from Wako Pure Chemical Industries, Ltd.) was slowly added to 2 g of MgO powder at room temperature. The mixture was then heated slowly to 140°C and kept at this reflux temperature for 2 h under stirring. The solid catalyst was washed several times with heptane and kept as suspension in anhydrous heptane under nitrogen.

Propylene polymerization

Propylene polymerization in slurry phase was performed in a 1 L stainless steel autoclave equipped with a mechanical stirrer. The reactor was repeatedly evacuated and purged with nitrogen several times to minimize residual oxygen and moisture. 200 ml of anhydrous heptane was introduced to the reactor under nitrogen flow. The solvent was then saturated with

propylene (donated by Japan Polypropylene Co., Ltd.) at 50ºC for 30 min, followed by the addition of 2.0 mmol of triisobutyl aluminum (TiBA, donated by Tosoh FineChem Co., Ltd.). 30 mg of catalyst in heptane was charged to the reactor to start polymerization. Semi-batch polymerization was carried out at 50ºC under 0.5 MPa of propylene pressure for 30 min before terminating by the addition of acidic alcohol. In separate experiments, propylene consumption profiles (termed as kinetic profiles) were recorded on a mass-flow meter for 2 h, where the polymerization conditions were the same with those described above except the fact that the polymerization was initiated by bomb injection of the catalyst.

Characterization

XRD was recorded on RINT 2100, Rigaku, using CuKα radiation at 40 kV and 30 mA in the 2è range of 5-85º with the scanning speed of 1º/min to identify and determine the crystallite structures and dimensions of MgO nano-crystals and $MgO/MgCl_2/TiCl_4$ catalysts. In the case of $MgO/MgCl_2/TiCl_4$ catalysts, the samples were prepared in a glove bag and sealed with Mylar film to minimize the contact with air and moisture. The crystallite size of MgO was calculated using the Scherrer equation: $d = K\lambda/B\cos\grave{e}$, where K is 0.94 for cubic dimensional crystal[13] and B is the full width at half maximum (FWHM) of the (200) diffraction peak. Transmission electron microscope (TEM) was recorded on Hitachi H-7100, operated at the accelerating voltage of 120 kV, to observe the morphology and estimate the particle size of MgO nano-crystals. Nitrogen adsorption/desorption experiments were conducted on Belsorp-max at 77 K and the surface area was calculated based on the BET method. The α_S-plot[14] was constructed from the adsorption volume ($V_{ads}(p/p_0)$) normalized at $V_{ads}(0.4)$ for a reference material (given later). The discrete adsorption data for the reference were numerically interpolated to generate a

continuous α_S axis. XPS was measured on Kratos AXIS-ULTRA DLD using monochromated Al-Kα radiation as the X-ray source. The anode was operated at 10 kV and 15 mA in an ultrahigh vacuum chamber maintained at the pressure below 5×10^{-9} Torr. A catalyst sample was transferred to the chamber using an air-tight transfer vessel. The neutralizer was used to reduce the charging effect to obtain better signal to noise ratio. The bulk titanium content of the $MgO/MgCl_2/TiCl_4$ model catalysts was analyzed by titration method. A catalyst sample was dissolved in H_2SO_4/HCl (aq) before the addition of excess aluminum beads to reduce Ti^{4+} into Ti^{3+}. The titration was performed using $Fe_2(SO_4)_3$ in H_2SO_4 (aq) as titrant in the presence of NH_4SCN as an indicator. The stereostructure of obtained polypropylene was analyzed by ^{13}C NMR (Bruker 400 MHz NMR spectrometer) at 120ºC using 1,1,2,2-tetrachloroethane-d_2 as an internal lock and reference.

3. Results and Discussion

$MgO/MgCl_2/TiCl_4$ core-shell catalysts with different surface areas were prepared by utilizing MgO nanoparticles having different sizes as the core material as described in our previous work.[11] Briefly, magnesium oxalate was calcined at different temperatures. The resultant MgO (**MgO1-5**) exhibited a cubic crystal structure in XRD, where the diffraction peaks became narrower for a lower calcination temperature. The crystal size estimated from the (200) diffraction peak of MgO using the Scherrer equation was in the range between 8 nm to 32 nm, depending on the calcination temperature as summarized in Table 1. TEM images in Figure 1 illustrated that all MgO samples have either a cubic or polygonal shape with the sizes almost the same as the crystal sizes obtained in XRD. The surface area analyzed by the BET

method increased with the decrease of particle size and the maximum surface area was found to be 221.5 m^2/g for **MgO5**, having the smallest particle size of 8 nm. The absence of intra-particle porosity for all the samples was validated by three different approaches; XRD analysis, TEM observation and particle size calculation from the BET surface area. Principally, particle size analysis from the BET surface area under the assumption of a cubic shape coincided well with the sizes obtained from crystallographic analysis by XRD and direct visualization by TEM, except for **MgO1**, which exhibited the BET-based size much larger than the other two sizes. This deviation for **MgO1** arose from the assumption of the cubic shape. Indeed, the assumption of a spherical shape resulted in a smaller BET-based size, indicating that **MgO1** has an intermediate shape between cubic and spherical, *i.e.* polygonal, in accordance with the TEM observation. The concurrence of the three different sizes indicated that the MgO samples are of single crystal and free from internal pores. Thus obtained MgO nano-crystal with well-defined structures was treated with $TiCl_4$, leading to the formation of $MgCl_2$ overlayer containing $TiCl_4$. As shown in Figure 2, minor and broad peaks appeared after the chlorination at around 15º, 30-35º and 50º, which are typical for anhydrous δ-$MgCl_2$. On the other hand, the FWHM values of the diffraction peaks for MgO were hardly affected except for **MgO5**, indicating that the formed δ-$MgCl_2$ overlayer was negligibly thin compared with the particle sizes. For exceptional **MgO5**, the chlorination underwent deeply into the bulk and MgO was mostly converted into α-$MgCl_2$ (Figure 2), plausibly due to the penetration of $TiCl_4$ into the bulk of this smallest MgO. Whilst **MgO1-4/$MgCl_2$/$TiCl_4$** catalysts more or less kept their BET surface areas after the chlorination, the surface area of **MgO5/$MgCl_2$/$TiCl_4$** was greatly reduced (from 221.5 to 47 m^2/g) due to particle agglomeration. Figure 3 shows α_S-plots constructed from the nitrogen adsorption isotherms for the **MgO2-5/$MgCl_2$/$TiCl_4$**

catalysts using that of **MgO1/$MgCl_2$/$TiCl_4$** as reference. The linearity of the plots for all the samples revealed the absence of micropore filling up to p/p_0 =1 (*i.e.* α_S = 1). Especially, it was found that **MgO5/$MgCl_2$/$TiCl_4$** still kept the non-porous feature in spite of the severe agglomeration. The external surface areas of **MgO2-5/$MgCl_2$/$TiCl_4$** calculated from the gradients of the α_S-plots were all in good agreement with the BET surface areas (Table 1).

Propylene polymerization was conducted using the obtained catalysts. We found that the propylene polymerization activity of the agglomerated **MgO5/$MgCl_2$/$TiCl_4$** catalyst shared the same straight line with the non-agglomerated **MgO1-4/$MgCl_2$/$TiCl_4$** catalysts when plotted against the BET surface area (Figure 4). In order to endorse this fact, we have prepared a **MgO6/$MgCl_2$/$TiCl_4$** catalyst starting from **MgO6** calcined at 600°C, which also experienced deep chlorination and severe agglomeration, evidenced by great reduction if the BET surface area from 157 to 49 m^2/g. The propylene polymerization activity of **MgO6/$MgCl_2$/$TiCl_4$** also laid on the same line. Thus, it was concluded that the agglomeration of the nanoparticles as the building unit does not affect the indistinct correlation between the BET surface area and olefin polymerization activity, which holds as long as the catalyst particles are free from intra-particle porosity. Figure 6 shows the kinetic profiles of the propylene polymerization using **MgO4/$MgCl_2$/$TiCl_4$** and **MgO1/$MgCl_2$/$TiCl_4$** catalysts. The curves belonged to the so-called decay-type kinetics, showing the maximum activity at the initial timing followed by rapid deactivation. Moreover, when the polymer yields were estimated from the kinetic profiles at each polymerization time (Figure 7), the two catalysts showed linear relationships between the yield and the BET surface area at each polymerization time. Namely, the two kinetic profiles were totally scalable over 2 h, where the ratio of the BET surface areas of the two catalysts corresponded to the scaling constant.

In order to understand the chemical states of the $MgCl_2/TiCl_4$ catalytic overlayer, the XPS analysis was conducted. The surface chemical composition of the model catalysts (summarized in Table 2) showed that the Ti concentration increased with the increase of the original MgO surface area, in line with the bulk Ti content determined by the titration technique. The surface chloride content similarly increased with the increase of the surface area, suggesting that the chlorination occurred more deeply for smaller MgO nano-crystal. The presence of lattice O from MgO was still observable, suggesting that the formed $MgCl_2/TiCl_4$ overlayers were sufficiently below 2 nm in agreement with the XRD results. Nevertheless, one should keep in mind that the non-uniform chlorination of MgO surfaces would also lead to similar observation. The binding energy (BE) of Mg 2s became broader in the direction of higher BE when MgO was chlorinated (Figure 5), which indicated the co-presence of $MgCl_2$ and MgO near the surfaces. For the most deeply chlorinated **MgO5/$MgCl_2$/$TiCl_4$** catalyst, the Mg 2s BE value became almost identical to that for a co-ground $MgCl_2/TiCl_4$ catalyst. This result clearly demonstrated the chemical transformation of magnesium species due to the deep chlorination of **MgO5** at least over a few nm. The BE values of Ti 2p for the $MgO/MgCl_2/TiCl_4$ catalysts were slightly shifted but basically similar when compared with those of a co-ground $MgCl_2/TiCl_4$ catalyst (Table 3). This fact suggested that Ti species most likely exists as $TiCl_4$ that is bound to $MgCl_2$ via chlorine bridges rather than $TiCl_xO_{4-x}$ directly bound to MgO through oxygen bridges. Hence, the chemical states of the $MgCl_2/TiCl_4$ overlayers are very similar to those of a typical ZN catalyst ($MgCl_2/TiCl_4$).

^{13}C-NMR analysis of the obtained polymer followed by the two-site model analysis on the pentad sequences[15] showed that the $MgO/MgCl_2/TiCl_4$ core-shell catalysts yielded polypropylene whose stereostructural characteristics are typical for donor-free $MgCl_2/TiCl_4$

Ziegler-Natta catalyst: the *mmmm* fraction around 50 mol% with a relatively high *rrrr* sequence, as can be seen in the non-negligible presence of the chain-end controlled fraction (*i.e.* ($\omega < 1$)).[16,17] Furthermore, it must be noted that the stereostructures of polypropylene, which reflect the nature of the active sites, were not affected by the catalyst surface area. These results are consistent with the conclusion obtained in XPS. The response of the model catalysts to the addition of ethylbenzoate (EB) as external donor (Al/donor = 10) was also similar to that of a typical $MgCl_2/TiCl_4$ catalyst: the increase in the isospecificity (*i.e.* higher σ value) together with the reduction in the chain-end controlled fraction (*i.e.* higher ω value).[16,17]

Conclusion

Non-porous and non-fragmentable $MgO/MgCl_2/TiCl_4$ core-shell catalysts were exploited as model catalysts to uncover the correlation between support architectures and the olefin polymerization performance of heterogeneous Ziegler-Natta catalysts. The non-porous nature of the $MgO/MgCl_2/TiCl_4$ catalysts were evidenced by comparative size analyses based on TEM, XRD, and nitrogen adsorption and by the α_S-plot analysis. The analyses of XPS results and polymer stereostructures clarified that $MgCl_2/TiCl_4$ overlayers well modeled the surface chemistry of typical Ziegler-Natta catalysts, being ideal to explore impacts of support architectures on the polymerization performance. It was concluded that the BET surface area of the catalysts is a primary parameter for the propylene polymerization activity and its kinetic profile as long as the catalysts are poreless.

Thus, we have proved that the $MgO/MgCl_2/TiCl_4$ catalysts chemically represent

typical Ziegler-Natta catalysts, while its unique structural features offer an ideal and powerful system to address relationships between the polymerization performance and support architectures, which had been long unclarified.

Acknowledgement

The Authors appreciate Japan Polychem Co., Mitsui Chemicals, Inc., Sumitomo Chemical Co., Ltd., Toho Titanium Co., Ltd., and Tosho Finechem Co. for the donation of reagents.

References

[1] E. Albizzati, U. Giannini, G. Collina, L. Noristi, L. Resconi, in: E.P. Moore, Jr. (Ed.), Polypropylene Handbook, Hanser-Gardner Publications: Cincinnati, OH, **1996**, p. 11.

[2] E. J. Arlman, P. Cossee, *J. Catal*. **1964**, *3*, 99.

[3] D. Fregonese, S. Mortara, S. Bresadola, *J. Mol. Catal. A: Chem.* **2001**, *172*, 89.

[4] R. Credendino, J. T. M. Pater, A. Correa, G. Morini, L. Cavallo, *J. Phys. Chem. C* **2011**, *115*, 13322.

[5] V. Busico, R. Cipullo, G. Monaco, G. Talarico, M. Vacatello, J. C. Chadwick, A. L. Segre, O. Sudmeijer, *Macromolecules* **1999**, *32*, 4173.

[6] B. Liu, T. Nitta, H. Nakatani, M. Terano, *Macromol. Chem. Phys.* **2003**, *204*, 395.

[7] T. Taniike, M. Terano, *J. Catal.* **2012**, *293*, 39.

[8] R. Gerbasi, A. Marigo, A. Martorana, R. Zannetti, G. P. Guidetti, G. Baruzzi, *Eur. Polym. J.* **1984**, *20*, 967.

[9] A. Marigo, C. Marega, R. Zannetti, G. Morini, G. Ferrara, *Eur. Polym. J.* **2000**, *36*, 1921.

[10] T. Taniike, P. Chammingkwan, V. Q. Thang, T. Funako, M. Terano, *Appl. Catal. A*: *Gen.* **2012**, *24*, 437.

[11] T. Taniike, P. Chammingkwan, M. Terano, *Catal. Commun*. **2012**, *27*, 13.

[12] A. Kumar, J. Kumar, *J. Phys. Chem. Solids* **2008**, *69,* 2764.

[13] N. Rakmak, W. Wiyaratn, C. Bunyakan, J. Chungsiriporn, *Chem. Eng. J*. **2010**, *162*, 84.

[14] K. S. W. Sing, in: D.H. Everett, R. H. Ottewill (Eds.), Surface Area Determination, Butterworths, London, **1970**, pp. 25–42.

[15] Y. Inoue, Y. Itabashi, R. Chujo, Y. Doi, *Polymer* **1984**, *25*, 1640.

[16] K. Goto, T. Taniike, M. Terano, *Macromol. Chem. Phys.* **2013**, *214*, 1011.

[17] S. Takahashi, T. Wada, T. Taniike, M. Terano, *Catalysts* **2013**, *3*, 137.

[18] Y. Ding, G. Zhang, H. Wu, B. Hai, L. Wang,Y. Qian, *Chem. Mater*. **2001**, *13*, 435.

Figure/Scheme Captions

Figure 1. TEM images of MgO particles: (a) **MgO1**, (b) **MgO2**, (c) **MgO3**, (d) **MgO4** and (e) **MgO5**

Figure 2. XRD patterns of $MgO/MgCl_2/TiCl_4$ model catalysts: (a) **$MgO1/MgCl_2/TiCl_4$**, (b) **$MgO2/MgCl_2/TiCl_4$**, (c) **$MgO3/MgCl_2/TiCl_4$**, (d) **$MgO4/MgCl_2/TiCl_4$** and (e) **$MgO5/MgCl_2/TiCl_4$**

Figure 3. α_S-plots for $MgO/MgCl_2/TiCl_4$ model catalysts: (a) **$MgO1/MgCl_2/TiCl_4$**, (b) **$MgO2/MgCl_2/TiCl_4$**, (c) **$MgO3/MgCl_2/TiCl_4$**, (d) **$MgO4/MgCl_2/TiCl_4$** and (e) **$MgO5/MgCl_2/TiCl_4$**

Figure 4. Relationship between the catalyst surface area and propylene polymerization activity

Figure 5. Mg 2s binding energy of $MgO/MgCl_2/TiCl_4$ model catalysts

Figure 6. Kinetic profile of the propylene polymerization using **$MgO1/MgCl_2/TiCl_4$** and **$MgO4/MgCl_2/TiCl_4$**

Figure 7. Relationship between the catalyst surface area and polymerization yield at various polymerization times

Table 1. Characterization results for MgO nanoparticles and $MgO/MgCl_2/TiCl_4$ catalysts

Sample	Calcination temperature [°C]	MgO nanoparticles			$MgO/MgCl_2/TiCl_4$ catalyst	
		Crystal size in XRD[a)] [nm]	BET surface area [m^2/g]	Particle size in BET[b)] [nm]	BET surface area [m^2/g]	External surface area from α_S-plot [m^2/g]
MgO1	800	32.0 (30.3[c)])	32.6	51.4 (20.7[c)])	32.7	-
MgO2	750	19.5	72.9	23.0	99.8	99.2
MgO3	700	16.3	103.4	16.2	106.8	105.7
MgO4	650	12.8	128.7	13.0	148.5	150.9
MgO5	500	8.0	221.5	7.6	47.0	47.3

[a)] Based on the Scherrer equation for the (200) peak of MgO ($K = 0.94$ for cubic crystal).

[b)] Based on $d_p = 6\times10^3/S_{BET}\cdot\rho$ for cubic particles, where S_{BET} is the BET surface area and ρ is the density of MgO (3.58 g/cm^3).[18]

[c)] Assuming spherical particles.

Table 2. Chemical composition of $MgO/MgCl_2/TiCl_4$ catalysts and a typical $MgCl_2/TiCl_4$ catalyst prepared by co-grinding

Catalyst	Ti[a)] [mol%]	O[a)] [mol%]	Cl[a)] [mol%]	Mg[a)] [mol%]	Bulk Ti[b)] [wt%]
MgO1/$MgCl_2$/$TiCl_4$	1.92	31.42	12.06	54.00	0.88
MgO2/$MgCl_2$/$TiCl_4$	2.41	30.16	11.98	55.45	2.39
MgO3/$MgCl_2$/$TiCl_4$	5.94	24.06	19.44	50.01	6.16
MgO4/$MgCl_2$/$TiCl_4$	7.10	15.65	31.62	45.62	7.72
MgO5/$MgCl_2$/$TiCl_4$	11.03	14.11	36.14	38.72	9.16
Co-ground $MgCl_2/TiCl_4$	5.08	-	62.36	32.56	4.48

[a)] Surface chemical composition based on the XPS measurements.

[b)] Bulk Ti content based on the titration.

Table 3. Binding energy of Ti 2p for $MgO/MgCl_2/TiCl_4$ model catalysts and a typical $MgCl_2/TiCl_4$ catalyst prepared by co-grinding

Catalyst	$Ti_{2p3/2}$	$Ti_{2p1/2}$
$MgO1/MgCl_2/TiCl_4$	458.5	464.1
$MgO2/MgCl_2/TiCl_4$	458.5	464.2
$MgO3/MgCl_2/TiCl_4$	458.4	464.0
$MgO4/MgCl_2/TiCl_4$	458.8	464.4
$MgO5/MgCl_2/TiCl_4$	458.7	464.3
Co-ground $MgCl_2/TiCl_4$	458.9	464.5

Table 4. Stereoregularity of produced polypropylene determined by ^{13}C NMR and fitting parameters based on the two-site model analysis in the absence and presence of ethylbenzoate (EB)

	No external donor				With EB as external donor			
	mmmm [mol%]	σ	P_m	ω	*mmmm* [mol%]	σ	P_m	ω
MgO1/$MgCl_2$/$TiCl_4$	52.7	0.931	0.311	0.750	61.4	0.949	0.278	0.800
MgO2/$MgCl_2$/$TiCl_4$	49.4	0.926	0.317	0.722	59.4	0.945	0.267	0.787
MgO3/$MgCl_2$/$TiCl_4$	50.8	0.924	0.270	0.755	61.6	0.952	0.286	0.788
MgO4/$MgCl_2$/$TiCl_4$	50.0	0.934	0.349	0.698	64.5	0.955	0.266	0.810
MgO5/$MgCl_2$/$TiCl_4$	n/a	0.925	0.254	0.749	63.4	0.957	0.278	0.792

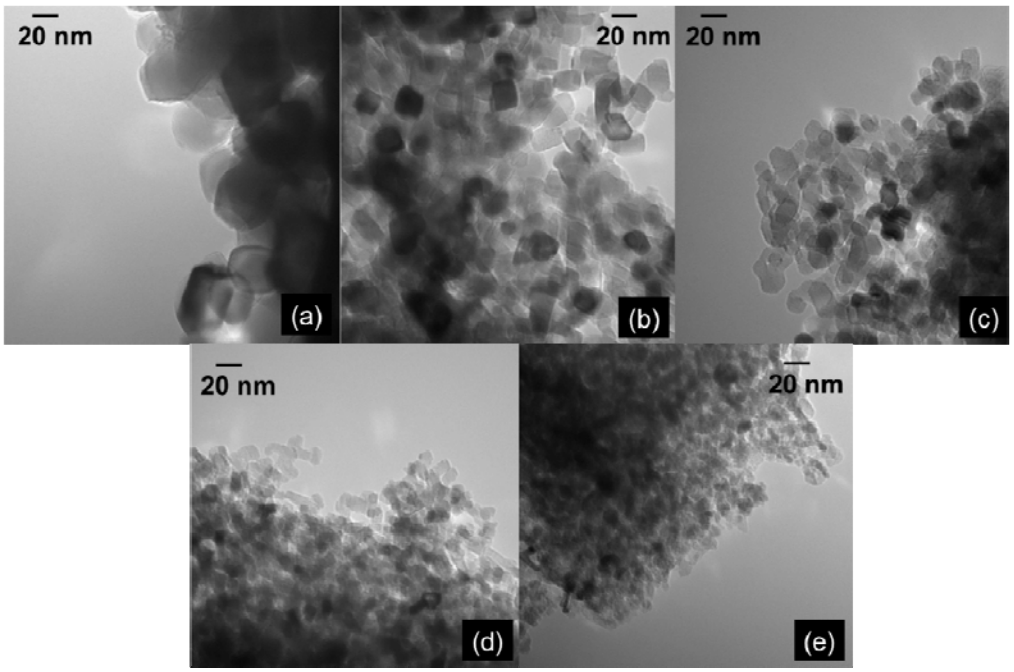

Figure 1. Chammingkwan et al.

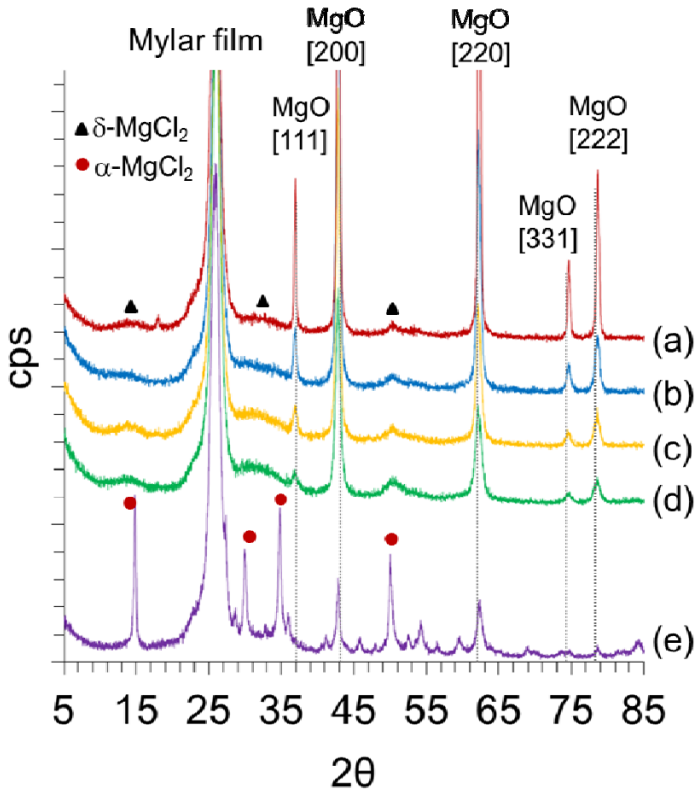

Figure 2. Chammingkwan et al.

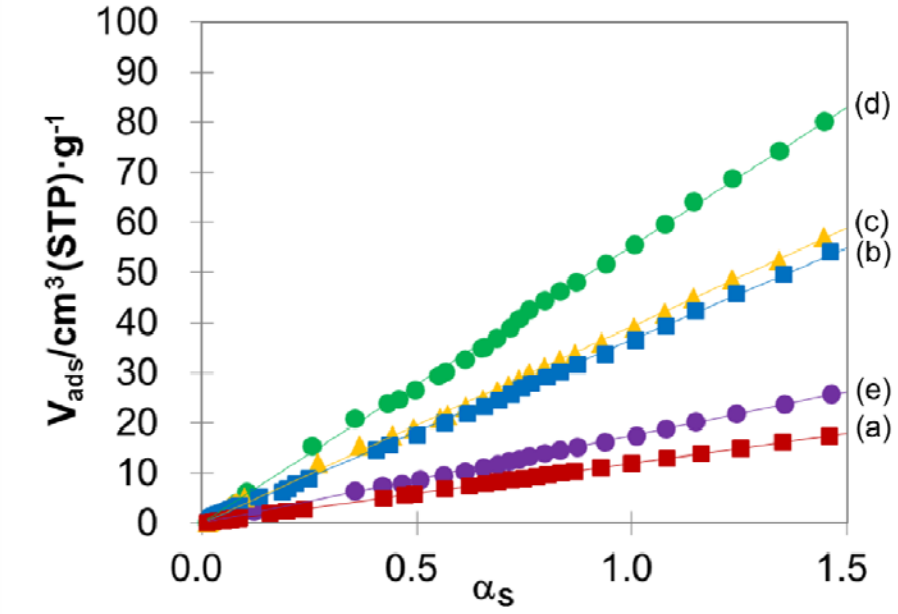

Figure 3. Chammingkwan et al.

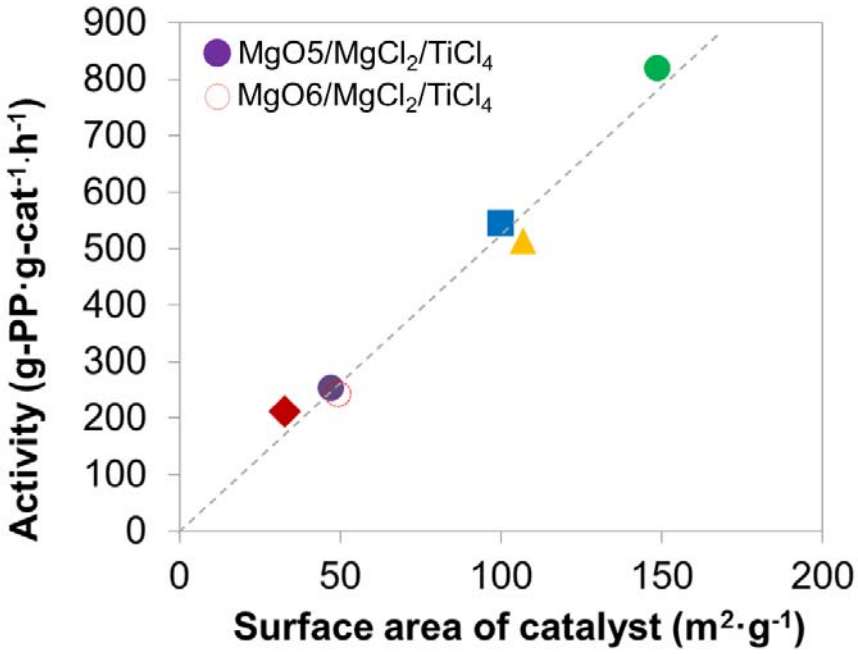

Figure 4. Chammingkwan et al.

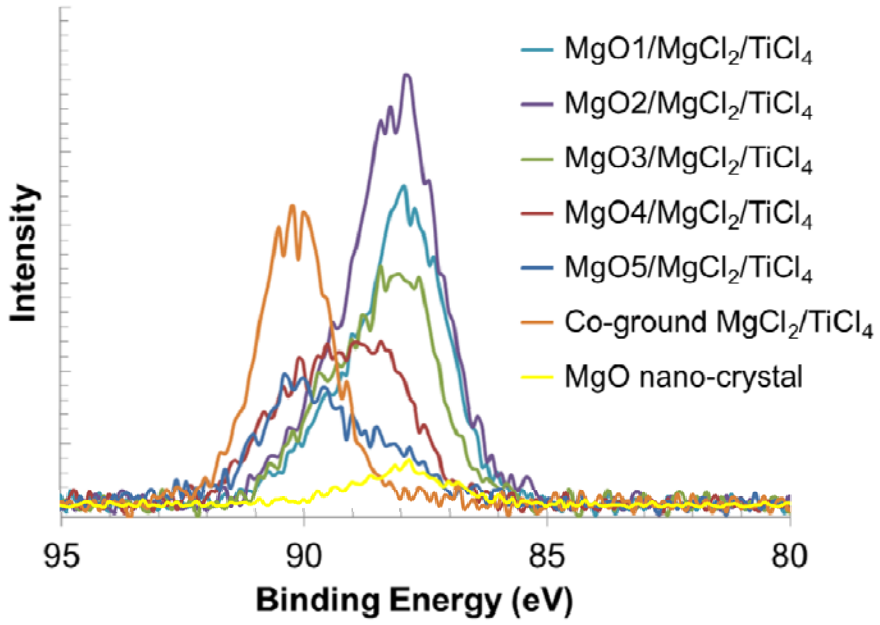

Figure 5. Chammingkwan et al.

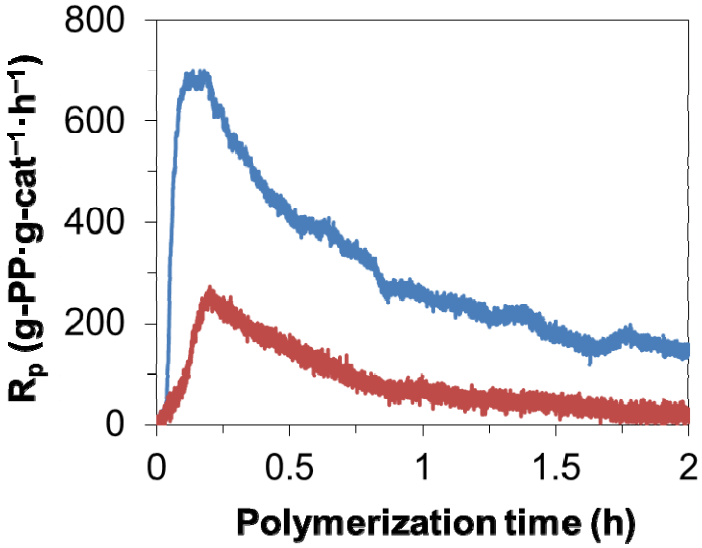

Figure 6. Chammingkwan et al.

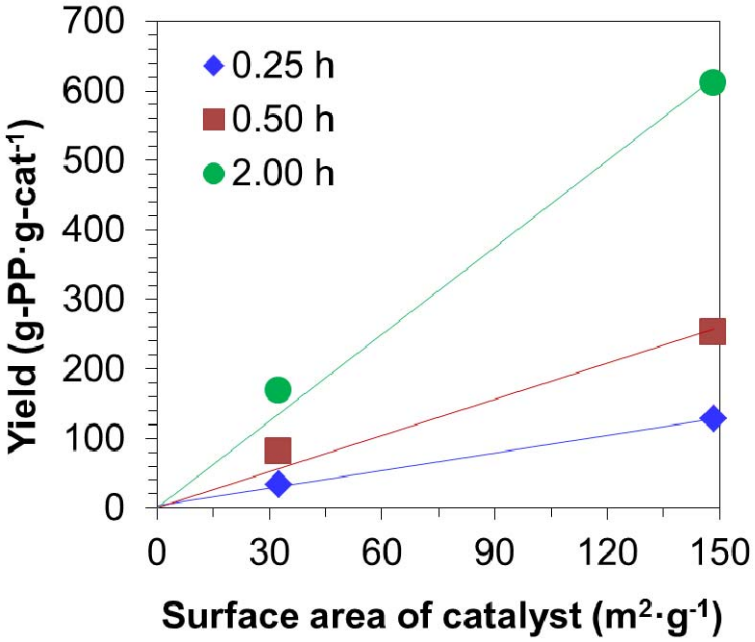

Figure 7. Chammingkwan et al.

Table of content

Unique structure of $MgO/MgCl_2/TiCl_4$ core-shell catalysts but yet identical surface chemistry with typical Ziegler-Natta catalyst offers an ideal and powerful tool to address relationships between the support architectures and polymerization performance.